NAMT
93-031

The Hysteretic Event in the Computation of Magnetization and Magnetostriction

David Kinderlehrer
Ling Ma
Carnegie Mellon University

Research Report No. 93-NA-031

October 1993

Sponsors

U.S. Army Research Office
Research Triangle Park
NC 27709

National Science Foundation
1800 G Street, N.W.
Washington, DC 20550

The hysteretic event in the computation of magnetization and magnetostriction

David Kinderlehrer and Ling Ma

Department of Mathematics and Center for Nonlinear Analysis
Carnegie Mellon University
Pittsburgh, PA. 15213-3890

1. Introduction Recent efforts to simulate magnetic and magnetostrictive processes have led to computations displaying marked hysteresis[1,2]. Our objective is to understand this computational event and this is a preliminary report about our efforts. A characteristic of the hysteretic cycle is that the system does not always assume a minimum energy state. Theories and models of hysteresis (cf. [24], [35] for compendia of these), pose rules to describe the paths hysteresis follow, but not why hysteresis occurs. Basics of Preisach modeling, for example, are explained there and in Mayergoyz [25] and Wiesen and Charap [39]. This type of phenomenological modeling is very useful in complex systems. It may accomodate domain wall motion and active constraints whose precise behavior at the microstructural level is extremely complicated.

Our objective is to understand the reason for hysteresis in the computation, although our approach is not conventional. Many qualitative explanations are available for this behavior. For example, friction or viscosity driven mechanisms which require rate equations and frequently enforce collapse of the hysteresis loop when the velocity tends to zero. However in the type of process we are discussing here, the hysteresis loop does not depend on the rate of traversal. Assuming the system navigates a path through local minima is another common mechanism. Evolution of such a system respects its own topological notions which need not be our own.

The propensity of optimization procedures to become marooned at local extrema when applied to nonconvex situations presents fundamental difficulties. A complicated potential well

[1] Supported by AFOSR 91 0301 and NSF DMS 911572 and by the ARO and the NSF through the Center for Nonlinear Analysis at Carnegie Mellon University.
[2] To appear in Proc. Nonlinear Diff. Eqns. and their Appl., College de France Sem, Brezis, H. and Lions, J.-L., eds.

structure and loading or other energetic contributions may compete, driving the system to develop mesh scale oscillations which need not be consistent with the grid. The computation of microstructure based on continuum theory is one area where these problems have been confronted [5,6,7,8,21,22,23,30].

Owing to the size and nonconvexity of the discretized problem, we are led to view the computation as an event, determine what it does, and attempt to model it, as it were, with a simpler system, a shadow system with a reduced number of dependent variables. Our success will then be measured by how well we are able to predict features of the computation, much as if we were conducting experiments on a physical system. What insight we achieve we can then hope to use in a discussion of the precise numerics.

In applying this approach, we first questioned whether or not we witnessed a systematic predictable event or whether we made an error either in the adoption of our computational method or in its execution. To test this, we computed our results for several decades of mesh refinements, finding nearly identical hysteresis curves. We then derived analytically a mesh independent estimate, explained below in §5, for the critical field encountered along the easy axis. Our estimate gives excellent agreement with our computations in the case of uniaxial anisotropy energy and fair agreement, with about 10% error, in the case of cubic anisotropy.

A central feature of our computations is the manner in which the system navigates from one state to its successor. Here we observe that successive states are not necessarily close either in uniform topology or in energy. The system undergoes very large variations which are spatially localized This bears a great resemblence to the weak topology.

Recent related thoughts about hysteretic behavior, principally in shape memory or pseudoelastic materials, may be found in Ball, Chu, and James [1], Bruno, Leo, and Shields [2], Fedelich and Zanzotto [11], Müller [26], Müller and Xu [27], Ortin [33], who explains his experiments by a Preisach model, and Sethna *et al.* [32] who exhibit computational results based on random hamiltonians. We note in §7 that we have computed hysteresis for models of some of these materials also. Keane and Rogers [19] have recently produced some interesting computations. A conceptually different approach to the computation of magnetic hysteresis is given by Giles, Alexopoulos, and Mansuripur [12].

2. Formulation We consider a two dimensional system governed by a magnetic anisotropy energy $\varphi(m)$ subjected to an external field H. This gives rise to a stored energy to which we add the energy of the induced magnetic field, sometimes referred to as the demagnetization energy, resulting in the functional

$$E(H,m) = \int_\Omega (\varphi(m) - H\cdot m)\, dx + \frac{1}{2}\int_{R^2} |\nabla u|^2\, dx, \qquad (2.1)$$

with

$$\operatorname{div}(-\nabla u + m\chi_\Omega) = 0, \quad |m| = 1 \text{ in } \Omega.$$

The second equation embodies Maxwell's equations for magnetostatics. The constraint on the magnetization m represents the requirement that the material be magnetically saturated. The domain Ω is the region occupied by the magnet. Typical forms for φ are

$$\varphi(m) = \kappa (m_2)^2 \qquad \text{(uniaxial)} \tag{2.2}$$

$$\varphi(m) = \kappa (m_1 m_2)^2 \qquad \text{(cubic)} \tag{2.3}$$

In the uniaxial case, when $\kappa > 0$, e_1 is the easy axis and when $\kappa < 0$, e_2 is the easy axis. In the cubic case, when $\kappa > 0$, e_1 and e_2 are easy axes and when $\kappa < 0$, $e_1 \pm e_2$ are easy axes. We shall restrict our attention to $\kappa > 0$.

Our computational technique applies equally well to linear magnetostriction, cf. Clark [4]. A major reason for studying both rigid magnets and linear elastic ones is to gain experience useful to analyze highly magnetostrictive materials, cf. [13,14,15,16,17] and [18] for an introductory account. In two dimensional linear magnetostriction, the material is endowed with a stored energy $\varphi(\varepsilon,m)$ which has the form

$$\varphi(\varepsilon,m) = \varphi_{el}(\varepsilon) + \varphi_{el/mag}(\varepsilon,m) + \varphi_{an}(m),$$

$$\varepsilon = \tfrac{1}{2}(\nabla y + \nabla y^T), \quad |m| = 1.$$

The elastic energy $\varphi_{el}(\varepsilon)$ is a typical linear elastic energy with cubic symmetry or lower. The elastic/magnetic interaction has the form

$$\varphi_{el/mag}(\varepsilon,m) = \sum b_{ij}\, \varepsilon_{ij}\, m_i m_j .$$

Note that it is even in m. The anisotropy energy $\varphi_{an}(m)$ is given by (2.2) or (2.3). The analogue of (2.1) is

$$E(H,y,m) = \int_\Omega (\varphi(\varepsilon,m) - m\cdot H)\, dx + \frac{1}{2}\int_{R^2} |\nabla u|^2\, dx. \tag{2.3}$$

Although we have computed (2.3) for magnetostriction, we have not as yet obtained any estimates which include the effects of elasticity.

For minimum energy at given H, one seeks

$$\inf_{\{|m| = 1\}} E(H,m) \quad \text{or} \quad \inf_{\{|m| = 1\}} E(H,y,m) \quad \text{subject to boundary conditions.}$$

The presence of a hysteresis curve in the ensuing computation is evidence that minimum energy is not actually achieved. Nonetheless, it remains useful to know the relaxation of the energy E(H,m) or E(H,y,m). We have computed some cases of the latter with Chipot [3].

3. Description of hysteresis We describe the hysteretic event. The computational domain is a rectangle $\Omega = (-L,L) \times (0,1)$, usually with $L = 1$, and oriented so that the x_1 axis is an easy direction. We partition Ω into $N_1 \times N_2$ squares of side length $h = 2L/N_1 = 1/N_2$ denoted by

$$\Omega_{ij} = \{x \in \Omega: ih - L < x_1 < (i+1)h - L,\ jh < x_2 < (j+1)h\},$$

$i = 0, \ldots, N_1 - 1$, $j = 0,1,\ldots,N_2 - 1$. The minimization of (2.1) is approximated in the space A_h by the Polak-Ribière version of the conjugate gradient method [31,33] where

$$A_h = \{ m: m \text{ is constant on each } \Omega_{ij}, i = 0, \ldots, N_1 - 1,\ j = 0,1,\ldots,N_2 - 1\}.$$

The minimization algorithm requires the computation of energy and also the gradient of the energy with respect to the discrete variables for a given set of $m \in A_h$. We remark that the most expensive feature of these computations is the determination of the averages of ∇u on the cells Ω_{ij}, i.e.,

$$\overline{\nabla u}_{ij} = \frac{1}{h^2} \int_{\Omega_{ij}} \nabla u \, dx.$$

We refer to Luskin and Ma [21] for details.

The hysteresis diagram is computed by continuation of solutions with respect to increasing and decreasing the applied magnetic field. We restrict to the case $H = (H_1,0)$. For a given initialization μ, let $T(\mu)$ denote the computed magnetization for the functional (2.1). Let H_o be the maximum external field strength, n be a positive integer, and $\delta = 2H_o/n$. We simulate the hysteresis by this algorithm:

1. Initialize m, set $H = (H_o,0)$, and compute $m^0 = T(m)$.
2. For $k = 1,2,\ldots,n$, set $H^k = (H_o - k\delta,0)$ and compute $m^k = T(m^{k-1})$.
3. For $j = 1,2,\ldots,n$, set $H^j = (-H_o + j\delta,0)$ and compute $m^j = T(m^{j-1})$.

The shown diagrams in Figures 8 and 9 are the overlaid graphs of $(H^k, E(H^k,m^k))$ and $(H^j, E(H^j,m^j))$.

The configuration begins at an absolute minimum of energy, or nearly so, for a large value of H_o and remains in this state until H^k changes sign. For these values of H^k, $m^k \approx m^0$, which we refer to as the precursor magnetization. This precursor magnetization is quite close to e_1.

The system then traverses a metastable regime where it does not achieve minimum energy. Some small oscillations are observed in this regime. The metastable regime ends in a critical field

range which appears to be characterized by the condition that the precursor magnetization becomes unstable at the critical field, H_{cr},

$$E(H_{cr},m) \leq E(H_{cr},m^0) \quad \text{for appropriate } m.$$

In fact, it seems that the computation seeks to resolve the closure domains first. These are the boundary columns of the computational grid. We shall use this as the basis for our estimate of H_{cr}.

Near $H = H_{cr}$, the system suffers instability and witnesses rapid interior oscillations, the evolution of microstructural domain configurations, and finally resolution to a nearly uniform state of approximately absolute minimum energy. In this regime, the behavior of the system is analogous to the classical Stoner-Wohlfarth scenario [34], which we review below. We are seeking a better analysis of this. Müller and Xu [27] also observe a stable/ metastable / unstable/ stable sequence in the extension of shape memory ribbons. We do not see this behavior when the applied field H is parallel to the hardest axis, which is x_2 in the uniaxial case and $x_1 \pm x_2$ in the cubic case. Indeed, there is almost no hysteresis in the hard axis uniaxial situation.

Here we are discussing only the major loops of the system, which are the overlaid graphs mentioned above. We have also computed minor loops and the virgin magnetization curve.

4. The Stoner-Wohlfarth theory In their fundamental work, Stoner and Wohlfarth [34] studied the behavior of the homogeneously magnetized ellipsoid. They exploited the property, known to Dirichlet, that if the magnetization is a constant vector parallel to a principle axis of the ellipsoid Ω, then the solution of

$$\Delta u = \operatorname{div} m\chi_\Omega \text{ in } \mathbb{R}^3$$

is a linear function when restricted to Ω. In two dimensions, for example, with B the unit ball, it is easy to check that for u satisfying

$$\Delta u = \operatorname{div} \xi\chi_B \text{ in } \mathbb{R}^2, \ \xi \text{ constant},$$

we have that

$$\nabla u = \tfrac{1}{2}\xi \quad \text{and}$$

$$\tfrac{1}{2}\int_B \nabla u\cdot\xi \, dx = \tfrac{1}{2}\int_{R^2} |\nabla u|^2 \, dx = \tfrac{\pi}{4}|\xi|^2 . \tag{4.1}$$

So if m is constant and $|m| = 1$, the induced field energy in (2.1) is simply a constant. In the Stoner-Wohlfarth framework, the system is regarded as homogeneous with energy given by the function

$$f(H) = \inf_{|m| = 1} \{\varphi(m) - m \cdot H\} + \frac{1}{4} .$$

For $|H|$ sufficiently large, the unique minimizing magnetization is just $m = H/|H|$. They devised a method to decide when the minimizing magnetization was unique based on determining the points $m = (\cos\theta, \sin\theta)$ which are simultaneously critical points and inflection points of $\varphi(m) - m \cdot H$. This gives two simultaneous equations for H which may be laboriously solved. For the case of the uniaxial energy (2.2), the curve bounding the region where m is not unique, and hence susceptible to hysteretic motion, is the astroid

$$\left(\frac{H_1}{2\kappa}\right)^{2/3} + \left(\frac{H_2}{2\kappa}\right)^{2/3} = 1 .$$

In the case of the cubic energy (2.3) the bounding curve is more complicated, but nowadays such computations are easily executed by symbolic programs like Mathematica and Maple. Examples are offered in Figure 1 below.

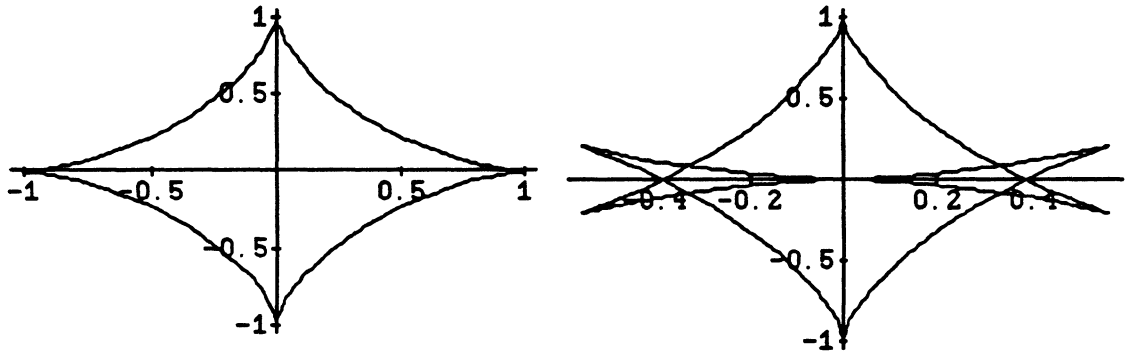

Figure 1.a. ParametricPlot[{Cos[t]^3,Sin[t]^3},{t,-Pi,Pi}] b. ParametricPlot[{-4Cos[4t]Cos[t] Sin[4t]Sin[t], Cos[t]Sin[4t] 4Cos[4t]Sin[t]},{t,-Pi,Pi}]

The Stoner - Wohlfarth curves for the uniaxial energy (2.2) and the cubic energy (2.3), a and b. The regions of the $H = (H_1,H_2)$ plane enclosed by the curves are where hysteretic behavior may occur.

Returning to the uniaxial situation, following the easy axis, choosing $H = (H_1,0)$, and starting with large positive H_1, we see that $m = e_1$ is an absolute minimum for $H_1 \geq 0$, it is stable for $-2\kappa \leq H_1 < 0$, and unstable for $H_1 < -2\kappa$. In the region $H_1 \leq 0$, the absolute minimum is attained by $-e_1$. We have drawn in Figure 2 the absolute and relative minimizing energy curves obtained by following a cycle from $(H_o,0)$ to $(-H_o,0)$ and returning to $(H_o,0)$. The critical field is $H_{cr} = 2\kappa$. We refer to this value as the Stoner-Wohlfarth critical field.

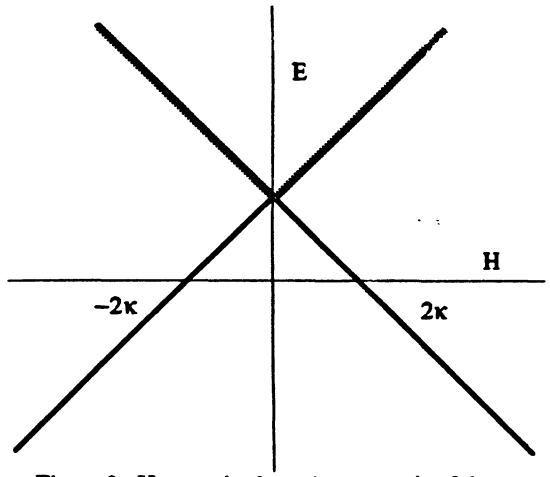

Figure 2. Hysteresis along the easy axis of the Stoner -Wohlfarth system.

An identical picture describes the system behavior for the cubic energy along the easy axis.

Hence the Stoner-Wohlfarth analysis gives a good cartoon of what we see in the computation, cf. Figures 8. The curve of minimum energy is different. It is not even the black Λ of Figure 2. This is because, as described in [13,14], fine phase laminates may result in homogeneous macroscopic magnetizations ξ with $|\xi| < 1$. More precisely, we may find a sequence $m^k \in L^\infty(\mathbb{R}^2;S^1)$ with

$$m^k \rightharpoonup \xi = (\xi_1,0) \quad \text{and} \quad E(H,m^k\chi_B) \to \tfrac{1}{4}\xi_1^2 - \xi_1 H_1 .$$

The expression for the limit energy on the right is minimized at $\xi_1 = 2H_1$ for $|H_1| < \frac{1}{2}$. DeSimone [9] has shown that the minimum is represented by the average magnetization ξ and results from the minimizing sequence $(m^k\chi_B)$ with

$$m^k(x) = \begin{cases} e_1 & \frac{j}{k} < x_2 < \frac{j}{k} + \frac{\lambda}{k} \\ -e_1 & \frac{j}{k} + \frac{\lambda}{k} < x_2 < \frac{j+1}{k} \end{cases} , \quad -\infty < j < \infty, \text{ and}$$

$$\lambda = \tfrac{1}{2}(2H_1 + 1).$$

We then have for $H = (H_1,0)$

$$E_{min}(H) = \begin{cases} -H_1^2 & |H_1| < \frac{1}{2} \\ -|H_1| + \frac{1}{4} & |H_1| \geq \frac{1}{2} \end{cases} ,$$

as shown for comparison in Figure 3.

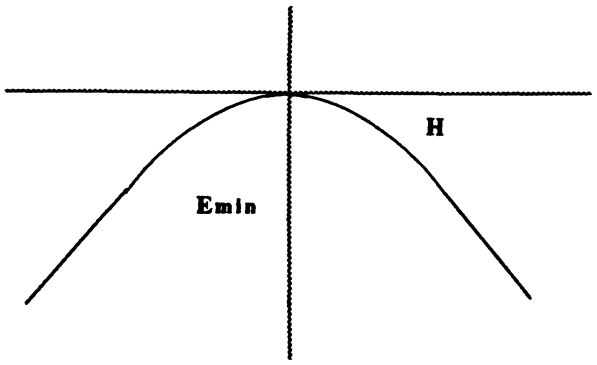

Figure 3. Sketch of minimum energy curve as applied field varies along an easy axis

5. Estimation of the critical field

We shall seek an estimate of the critical field described in §3 at which the system becomes unstable. We seek this estimate as a correction to the Stoner - Wohlfarth critical field value $H_{SW} = 2\kappa$. The most important feature of this estimate is that it is independent of the mesh size. Our estimate gives excellent agreement with our computations in the uniaxial case (2.2) and fair agreement in the cubic case (2.3). Later we discuss possible reasons for the difficulties with the cubic case.

The general procedure in the analytical investigation is to replace the system by a simpler shadow system. The energy for the shadow system (2.1) is an effort to account for the effect of the demagnetization energy in a more general region than a disc and is derived under two approximations. Suppose that the computational domain is a rectangle $\Omega = (-L,L) \times (0,1)$ with $L = Nh$. We shall assume that

a) the magnetization m is constant in each column, and

b) the coupling of m in a column with the field is approximated by a line integral times the width of the column.

To merely estimate the critical field, it is not necessary to introduce all of this apparatus, but instead it is sufficient to impose a criterion. This criterion is that the computation first seeks to resolve the closure domains, the first and last columns of the computational domain and that at this field value, the precursor magnetization m_o loses stability. Moreover, in the shadow system the precursor magnetization is actually e_1, which we assume as well in our computation below. This condition may be justified [20]. Assume that φ is an anisotropy energy with easy axis e_1. This leads to the condition

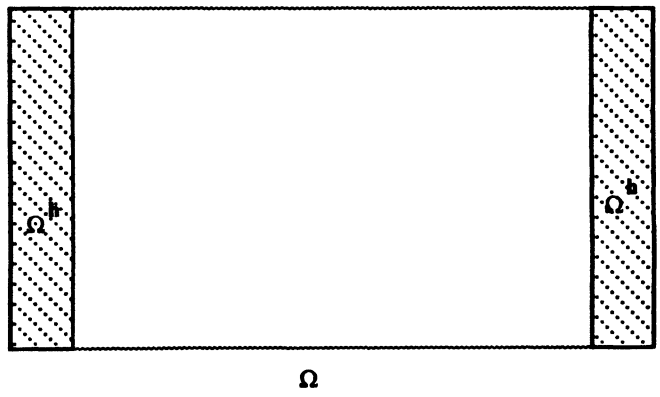

Figure 4. The computational region with the closure domain Ω^h.

$$E(H,m) \le E(H,e_1) \quad \text{for all } m \text{ with } m|_{\Omega\setminus\Omega^h} = e_1,$$

$$H = (-H_{cr},0),\ H_{cr} \ge 0, \tag{5.1}$$

$$\Omega^h = \text{first and last columns of } \Omega.$$

Denote by w a function satisfying

$$w \in H^1_{loc}(\mathbb{R}^2):\ \Delta w = \frac{\partial}{\partial x_1}\chi_\Omega \quad \text{in } \mathbb{R}^2. \tag{5.2}$$

From (5.1), we have that

$$\int_\Omega (\varphi(m) - H\cdot m)\,dx + \frac{1}{2}\int_{\mathbb{R}^2} |\nabla u|^2\,dx \le -\int_\Omega H\cdot e_1\,dx + \frac{1}{2}\int_{\mathbb{R}^2} |\nabla w|^2\,dx.$$

We write

$$m = \begin{cases} \xi & \text{in } \Omega^h \\ e_1 & \text{in } \Omega\setminus\Omega^h \end{cases},\ |\xi| = 1, \tag{5.3}$$

so that

$$\int_{\Omega^h} \varphi(\xi)\,dx - \frac{1}{2}\int_{\mathbb{R}^2} \{|\nabla w|^2 - |\nabla u|^2\}\,dx \le \int_\Omega H\cdot(m - e_1)\,dx$$

whence

$$\int_{\Omega^h} \varphi(\xi)\,dx - \frac{1}{2}\int_{\mathbb{R}^2} \{|\nabla w|^2 - |\nabla u|^2\}\,dx \le H_{cr}\int_{\Omega^h} (1 - \xi_1)\,dx.$$

We express the field energies as an integral over Ω^h by writing

$$\begin{aligned}\int_{\mathbb{R}^2} \{|\nabla w|^2 - |\nabla u|^2\}\,dx &= \int_{\mathbb{R}^2} \nabla(w+u)\cdot\nabla(w-u)\,dx \\ &= \int_\Omega \nabla(w+u)\cdot(e_1 - m)\,dx \\ &= \int_{\Omega^h} \nabla(w+u)\cdot(e_1 - \xi)\,dx\end{aligned}$$

Hence

$$\int_{\Omega^h} \varphi(\xi)\,dx - \frac{1}{2}\int_{\Omega^h} \nabla(w+u)\cdot(e_1 - \xi)\,dx \le H_{cr}\int_{\Omega^h} (1 - \xi_1)\,dx.$$

We restrict magnetization variations to ξ = constant in Ω^h. Writing $u = u^{(h)}$ to denote the dependence of u on Ω^h, we now have that

$$\varphi(\xi) - \frac{1}{2}\int_{\Omega^h} \nabla(w + u^{(h)})\cdot(e_1 - \xi)\,dx \le (1-\xi_1)H_{cr}$$

or

$$\max_{\xi}\left\{\frac{\varphi(\xi)}{1-\xi_1} - \frac{1}{1-\xi_1}\frac{1}{2}\int_{\Omega^h} \nabla(w + u^{(h)})\cdot(e_1 - \xi)\,dx\right\} \le H_{cr}. \qquad (5.4)$$

In order to evaluate the integral in (5.4), we use some facts about w and $u^{(h)}$. Given a region A, let w_o, w_1, and w_2 denote the solutions of

$$\Delta w_o = \chi_A \quad \text{in } \mathbb{R}^2 \text{ and}$$

$$\Delta w_j = \frac{\partial}{\partial x_j}\chi_A \quad \text{in } \mathbb{R}^2,\ j = 1,2. \qquad (5.5)$$

It is easy to check that $w_j = \frac{\partial}{\partial x_j} w_o$ and hence

$$\operatorname{div}(w_1,w_2) = \chi_A \quad \text{and} \quad \operatorname{curl}(w_1,w_2) = 0 \quad \text{in } \mathbb{R}^2. \qquad (5.6)$$

We retain the notation $w = w_1$ for $A = \Omega$ and introduce

$$w_1 = w_1^{(h)} \quad \text{and} \quad w_2 = w_2^{(h)} \quad \text{for } \Omega^h. \qquad (5.7)$$

Now $u^{(h)}$ is the solution of

$$\Delta u^{(h)} = \operatorname{div} m\chi_\Omega$$

$$= \operatorname{div} e_1\chi_\Omega + \operatorname{div}(\xi - e_1)\chi_{\Omega^h}.$$

Thus we may write

$$u^{(h)} = w + (\xi_1 - 1)w_1^{(h)} + \xi_2 w_2^{(h)},$$

$$w + u^{(h)} = 2w + (\xi_1 - 1)w_1^{(h)} + \xi_2 w_2^{(h)}, \text{ and}$$

$$\nabla(w + u^{(h)})\cdot(e_1 - \xi) = 2(1-\xi_1)\frac{\partial w}{\partial x_1} - (1-\xi_1)^2\frac{\partial w_1^{(h)}}{\partial x_1} - \xi_2^2\frac{\partial w_2^{(h)}}{\partial x_2}$$

$$+ 2\xi_2\frac{\partial w}{\partial x_2} - \xi_2(\xi_1 - 1)\frac{\partial w_1^{(h)}}{\partial x_2} + \xi_2(1-\xi_1)\frac{\partial w_2^{(h)}}{\partial x_1}.$$

We rewrite this expression using (5.6). Before performing this reduction, note that for $A = \Omega$ or Ω^h, $w_o(x) = w_o(x_1, 1-x_2)$. This also holds for w_1. This symmetry property implies that

$$\int_{\Omega\cap\{x_1 = a\}} \frac{\partial w_1}{\partial x_2}\,dx_2 = 0. \qquad (5.8)$$

Thus

$$\nabla(w + u^{(h)})\cdot(e_1 - \xi) = 2(1-\xi_1)\frac{\partial w}{\partial x_1} - (1-\xi_1)(2\xi_1\frac{\partial w_1^{(h)}}{\partial x_1} - (1+\xi_1)) + I,$$

where by (5.8),

$$\int_{\Omega^h} I\,dx = 0.$$

Our task now is to estimate the expression

$$\gamma^{(h)} = \frac{1}{1-\xi_1}\frac{1}{2}\int_{\Omega^h}\nabla(w + u^{(h)})\cdot(e_1 - \xi)\,dx$$

$$= \int_{\Omega^h}\left\{\frac{\partial w}{\partial x_1} - (\xi_1\frac{\partial w_1^{(h)}}{\partial x_1} - \frac{1}{2}(1+\xi_1))\right\}dx\,. \tag{5.9}$$

Instead, we estimate $\gamma^{(o)} = \lim_{h\to 0}\gamma^{(h)}$. Our first expression for $\gamma^{(o)}$ is

$$\gamma^{(o)} = \int_{\Gamma_1}\left\{\frac{\partial w}{\partial x_1} - (\xi_1\frac{\partial w_1^{(o)}}{\partial x_1} - \frac{1}{2}(1+\xi_1))\right\}dx_2\,. \tag{5.10}$$

To pursue this estimate, we need additional information about w and $w_1^{(h)}$.

First, we shall need a formula for

$$\frac{\partial w_1}{\partial z} = \frac{\partial w_1}{\partial x_1} - i\frac{\partial w_1}{\partial x_2} \quad \text{for} \quad z \in A.$$

This is available from the Plemelj Formulas, cf. Muskhelishvili [28], and is given by

$$\frac{\partial w_1}{\partial z}(z) = \frac{1}{2\pi i}\int_{\partial A}\frac{1}{t-z}(\nu_1 - i\nu_2)\nu_1\,dt, \tag{5.11}$$

where $\nu = (\nu_1,\nu_2)$ is the exterior normal to ∂A. The determination of (5.11) clearly utilizes the jump relations implicit in (5.5).

We specialize to $A = \Omega$ and $A = \Omega^h$. For Ω, we see that

$$\frac{\partial w_1}{\partial z}(z) = \frac{1}{2\pi i}\int_{\Gamma_1}\frac{1}{t-z}dt + \frac{1}{2\pi i}\int_{\Gamma_2}\frac{1}{t-z}dt \quad , z \in \Omega, \tag{5.12}$$

where $\Gamma_1 = \{ x_1 = L, 0 < x_2 < 1 \}$ and $\Gamma_2 = \{ x_1 = -L, 0 < x_2 < 1 \}$. The real parts of these terms merely describe the increment of the angle of z as the arcs are traversed and results in the

sum of the angles subtended by z and the segments Γ_1 and Γ_2. We obtain in this fashion the formula

$$\frac{\partial w_1}{\partial z}(z) = \frac{1}{2\pi}(\theta_1(z) + \theta_2(z)) - i\frac{\partial w_1}{\partial x_2}(z), \quad z \in \Omega, \tag{5.13}$$

where $\theta_j(z)$ are depicted in Figure 5. From this it follows in particular that

$$\lim_{z \to \Gamma_1} \frac{\partial w_1}{\partial x_1}(z) = \frac{1}{2} + \frac{1}{2\pi}\theta_2(z)\,. \tag{5.14}$$

We shall evaluate $\theta_2(z)$ precisely later on.

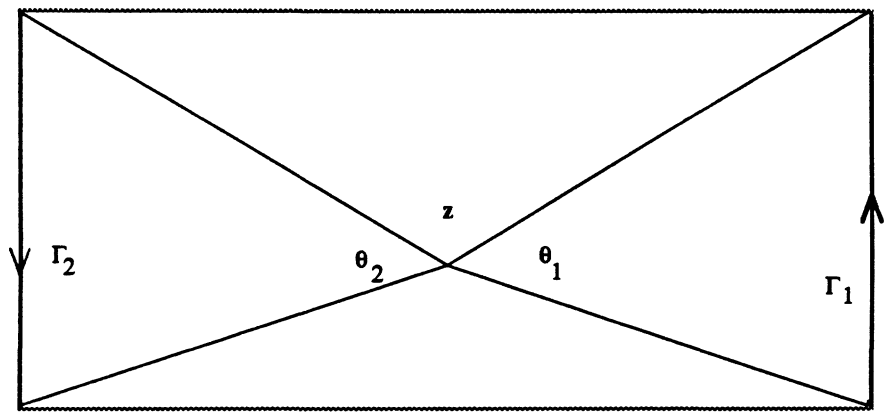

Figure 5. The angles θ_1 and θ_2 subtended by z and the arcs Γ_1 and Γ_2, cf. (5.12) and (5.13).

Specializing now to Ω^h, we have for $w_1 = w_1^{(h)}$,

$$\frac{\partial w_1^{(h)}}{\partial z}(z) = \frac{1}{2\pi i}\int_{C_1^h} \frac{1}{t - z}\,dt + \frac{1}{2\pi i}\int_{C_2^h} \frac{1}{t - z}\,dt \quad , z \in \Omega, \tag{5.15}$$

where C_1^h and C_2^h are the four segments indicated in Figure 6.

Figure 6. The four dark vertical segments comprise the contour of the integral in (5.15).

Again we recognize real part of (5.15) as the sum, with appropriate signs, of angles subtended by the segments which comprise the C_j^h. In particular,

$$\frac{\partial w_1^{(o)}}{\partial x_1}(z) = \lim_{h \to 0} \frac{\partial w_1^{(h)}}{\partial x_1}(z) = 1 \quad \text{for} \quad z \in \Gamma_1. \tag{5.16}$$

Returning now to (5.10),

$$\gamma^{(o)} = \tfrac{1}{2} + \int_{\Gamma_1} \frac{1}{2\pi}\theta_2(z)\, dx_2 + \tfrac{1}{2}(\xi_1 - 1) = \lambda + \tfrac{1}{2}(\xi_1 - 1), \tag{5.17}$$

with λ to be computed shortly. We now have

$$H_{cr} = \max_{\xi} \left\{ \frac{\varphi(\xi)}{1 - \xi_1} - \lambda + \tfrac{1}{2}(1 - \xi_1) \right\}. \tag{5.18}$$

For φ given by (2.2) or (2.3), this results in a domain dependent correction to the Stoner - Wohlfarth critical field of the form

$$H_{cr} = 2\kappa - \lambda, \quad \text{when} \quad \kappa \geq \tfrac{1}{2}. \tag{5.19}$$

The reader may easily check that

$$\int_{\Gamma_1} \frac{1}{2\pi}\theta_2(z)\, dx_2 = \frac{1}{2\pi}(4L) \int_0^{\frac{1}{2L}} \arctan \sigma \, d\sigma$$

$$= \frac{1}{\pi}\left(\arctan \frac{1}{2L} - L \log\left(1 + \left(\frac{1}{2L}\right)^2\right)\right),$$

resulting in $\lambda \approx 0.6$ when $L = 2$. This gives a predicted value for the critical field of

$$H_{cr} = 2\kappa - 0.6$$

6. Comparison with computation The table below summarizes our computational results. The data for both cases were taken from computations on a 16×8 grid but these were identical to the results from a 32×16 grid. In the uniaxial case the predicted value is nearly identical to the computed one. Samples of graphical renderings of the computations appear in Figures 8 - 11. The range of values of the anisotropy constant κ was chosen so the energy stored in a body of constant magnetization was comparable to the induced field energy. This is the case in common magnetic materials.

κ	H_{cr} (predicted)	uniaxial H_{cr} (computed)	cubic H_{cr} (computed)
1	1.4	1.6	1.3
1.2	1.8	1.8	1.7
1.4	2.2	2.3	2.1
1.6	2.6	2.6	2.3
1.8	3.0	3.0	2.6
2.0	3.4	3.4	3

Table 1. Tabulated comparison of predicted and computed critical fields

We suspect that the variation we see in the cubic case owes primarily to the inadequacy of $m_o = e_1$ to serve as a precursor magnetization. A better precursor magnetization in this case might be somewhat tilted from the x_1 - axis at the four corners of Ω. A version of the actual shadow energy in this situation is

$$E_{sh}(H,\xi) = E(H,e_1) + 2h\{\varphi(\xi) - (\xi_1 - 1)(H - \lambda) + \tfrac{1}{2}(\xi_1 - 1)^2\}.$$

Inspection of E_{sh} as a function of ξ for a range of values of H suggests that e_1 dwells in a more shallow well in the cubic case than in the uniaxial one.

Computations of (2.1) with field varying along a hard axis have also been attempted. Our preliminary results indicate that the computed and predicted applied fields at which the uniform magnetization loses stability are in good agreement.

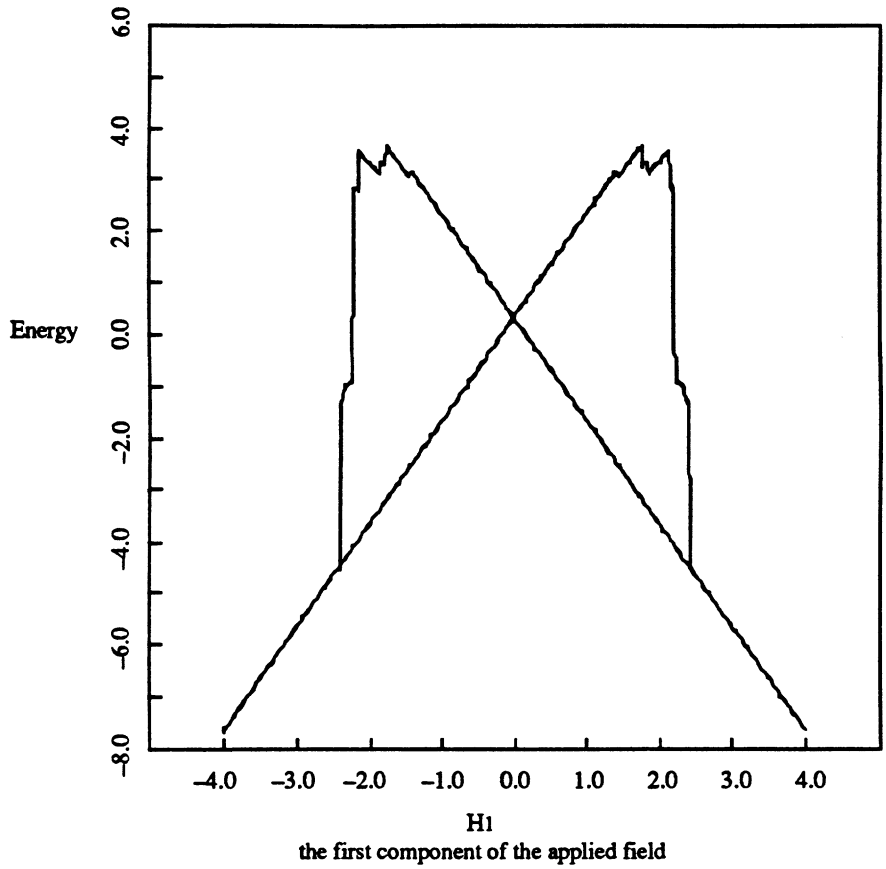

Figure 9. Computed hysteresis picture for cubic anisotropy energy (2.3) with $\kappa = 1.6$.

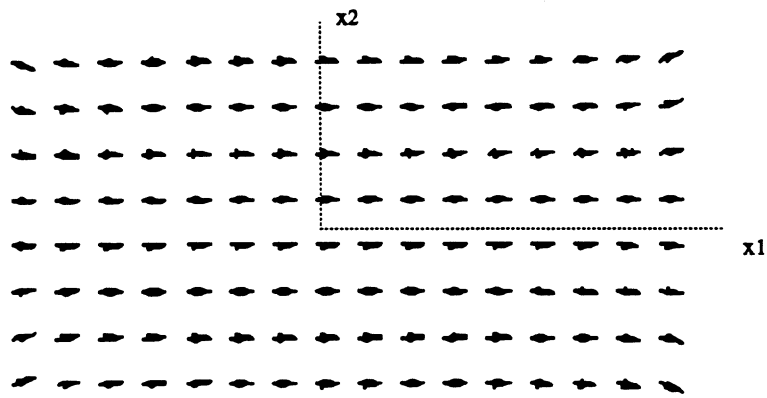

Figure 10. Computed magnetization configuration for uniaxial anisotropy energy (2.2) with $\kappa = 1.6$ at field value $H = (-2.1,0)$. This is in the metastable range.

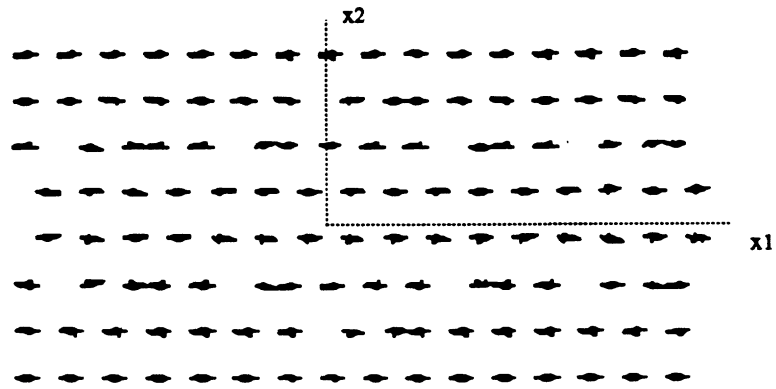

Figure 11. Computed magnetization configuration for uniaxial anisotropy energy (2.2) with $\kappa = 1.6$ at field value $H = (-2.32,0)$. This is in the unstable range.

7. Other systems Our conception is that most nonconvex computational optimization problems result in hysteretic behavior. As an example we have begun investigation of the Ericksen bar [10], which is a one dimensional version of a shape memory or pseudoelastic material. Hysteretic patterns of stress vs. load parameter in the extension of shape memory ribbons have been reported by Müller and Xu [27], as cited earlier, and by Ortin [30]. Their observations, while quite different, share certain features, in particular the sequence of states passing from stable to metastable to unstable. These experiments, in which the orientation of the sample was not recorded, suggest attempting a simulation in one space dimension with an energy density which is not convex. This amounts to studying the well known Ericksen bar. The computation becomes a one dimensional version of (2.1), without, however, the induced field energy. We reproduced the general features of the experiments, but further investigation is necessary to understand if many details are also reproduced by our computations. Consideration of the shape memory ribbon as governed by a random hamiltonian has been studied by [32].

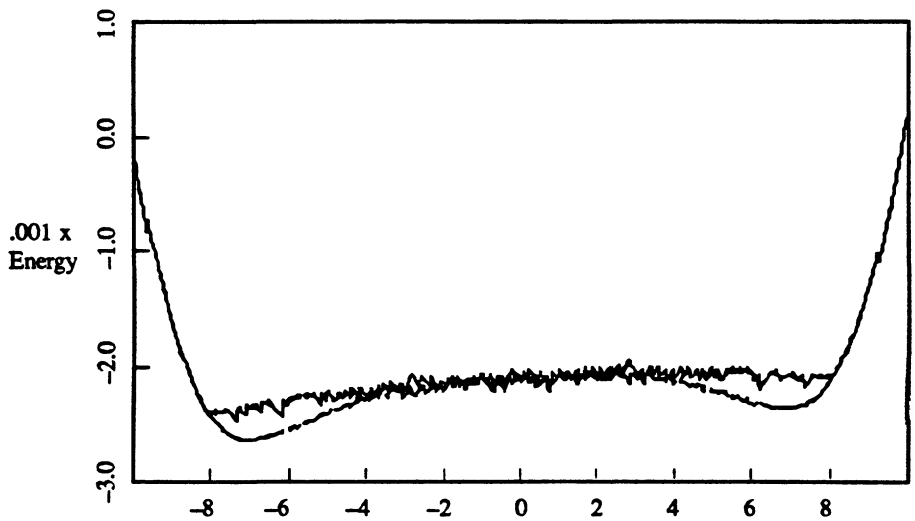

Figure 12. Computed hysteresis diagram for an Ericksen bar

For the example illustrated in Figure 12, we computed

$$E(\tau) = \int_0^1 \varphi(u')\,dx \quad \text{subject to} \quad u(0) = 1 \quad \text{and} \quad u(1) = \tau \tag{7.1}$$

using the format discussed in §3 with

$$\varphi(t) = t^2(t^2 - 100) + 20t. \tag{7.2}$$

Note that $\varphi(0) = 0$ suggesting that the computed configuration is rather close to the Maxwell line.

Acknowledgements We thank Richard James, Mitchell Luskin, Roy Nicolaides, and Jose Ortin for their interest and helpful suggestions.

References

[1] Ball, J. M.,Chu, C., and James, R. D. Metastability and hysteresis in elastic crystals (to appear)

[2] Bruno, O., Leo, P., and Shields, T. Transient heat transfer effects on the pseudoelastic behavior of shape-memory wires, Center for Nonlinear Analysis report 92NA040

[3] Chipot, M., Kinderlehrer, D., and Ma, L. to appear

[4] Clark, A. E. 1980 Magnetostrictive rare earth - Fe_2 compounds, *Ferromagnetic Materials, Vol 1* (Wohlfarth, E. P. ed) North Holland, 532 - 589

[5] Collins, C. and Luskin, M. 1989 The computation of the austenitic-martensitic phase transition, Lecture Notes in Physics 344 (ed. M. Rascle, D. Serre and M. Slemrod), Springer-Verlag, 34-50.

[6] Collins, C. and Luskin, M. Numerical modeling of the microstructure of crystals with symmetry-related variants, *Proc. ARO US-Japan Workshop on Smart/Intelligent Materials and Systems*, Technomic

[7] Collins, C. and Luskin, M. Optimal order error estimates for the finite element approximation of the solution of a nonconvex variational problem, to appear

[8] Collins, C., Kinderlehrer, D., and Luskin, M. 1991 Numerical approximation of the solution of a variational problem with a double well potential, SIAM J. Numer. Anal., 28, 321-333

[9] De Simone, A. 1992 Energy minimizers for large ferromagnetic bodies, thesis, Univ. Minn.

[10] Ericksen, J. 1975 Equilibrium of bars, J. Elasticity, 5, 191-201

[11] Fedelich, B. and Zanzotto, G. 1992 Hysteresis in discrete systems of possibly interacting elements with a double well energy, J. Nonlinear Sci., 2, 319-342

[12] Giles, R., Alexopoulos, P. S., and Manuripur, M. 1992 Micromagnetics of thin film cobalt-based media for magnetic recording, Comp. in Physics, 6, 53-70

[13] James, R. D. and Kinderlehrer, D. 1990 An example of frustration in a ferromagnetic material, Nematics: Mathematical and Physical Aspects, (Coron, J.-M., Ghidaglia, J.-M., and Hélein, F., eds), Kluwer NATO ASI series, 201-222

[14] James, R. D. and Kinderlehrer, D. 1990 Frustration in ferromagnetic materials, Cont. Mech. Therm., 2, 215-239

[15] James, R. D. and Kinderlehrer, D. 1992 Frustration and microstructure: an example in magnetostriction, *Prog Part Diff Eqns: calculus of variations, applications* (Bandle, C. et. al., eds) Pitman Res Notes Math 267, 59-81

[16] James, R. D. and Kinderlehrer, D. 1992 Twinned structures in terfenol, Proc. ICOMAT

[17] James, R. D. and Kinderlehrer, D. 1993 Mathematical approaches to the study of smart materials, *Mathematics in Smart Structures, Smart Structures and Materials '93*, Proceedings SPIE vol. 1919, (Banks, H. T., ed.) 2-18

[18] James, R. D. and Kinderlehrer, D. A theory of magnetostriction with application to $TbDyFe_2$ Phil. Mag. (to appear)

[19] Keane, M. K. and Rogers, R. C. A finite dimensional model problem in ferromagnetism, J. Int. Mat. and Struct. (to appear)

[20] Kinderlehrer, D., and Ma, L. to appear

[21] Luskin, M. and Ma, L. 1992 Analysis of the finite element approximation of microstructure in micromagnetics, SIAM J. Num Anal., 29, 320-331

[22] Luskin, M. and Ma, L. 1993 Numerical optimization of the micromagnetics energy, *Mathematics in Smart Structures, Smart Structures and Materials '93*, Proceedings SPIE vol. 1919, (Banks, H. T., ed.) 19-29

[23] Ma, L. 1993 Computation of magnetostrictive materials, *Mathematics in Smart Structures, Smart Structures and Materials '93*, Proceedings SPIE vol. 1919, (Banks, H. T., ed.) 47-54

[24] Ma, L. and Walkington, N. On algorithms for nonconvex optimization, to appear

[25] Macki, J. W., Nistri, P., and Zecca, P. 1993 Mathematical models for hysteresis, SIAM Review, 35, 94-123

[26] Mayergoyz, I. D. 1991 *The Preisach Model for Hysteresis*. Springer

[27] Müller, I. 1989 On the size of the hysteresis in pseucoelasticity, Cont. Mech. Therm., 1, 125-142

[28] Müller, I. and Xu, H. 1991 On the pseudoelastic hysteresis, Acta Metall., 39, 263-271

[29] Muskhelishvili, N. I. 1992 *Singular Integral Equations*, Dover (reprint of 1953 Noordhoff edition)

[30] Nicolaides, R. A. and Walkington, N. J. 1992 Computation of microstructure using Young measure representations, *Recent Advances in Adaptive and Sensory Materials and their Applications*, (Rogers, C. A. and Rogers, R. A., eds), Technomic, 1992

[31] Ortin, J. 1992 Preisach modeling of hysteresis for a pseudoelastic Cu-Zn-Al single crystal, J. Appl. Phys ,71,1454-1461

[32] Polak, E. 1971 *Computational methods in optimization* , Academic Press

[33] Sethna, J., Dahmen, K., Kartha, S., Krumhansl, J., Roberts, B. and Shore, J. Hysteresis and heirachies: dynamics of disorder-driven first-order phase transitions, to appear

[34] Stoer, J. and Bulisch, R. 1993 *Introduction to numerical analysis, 2nd edition*, Springer

[35] Stoner, E. C. and Wohlfarth, E. P. 1948 A mechanisim of magnetic hysteresis in heterogeneous alloys, Phil. Trans. Royal Soc. (London) Sect A, 240, 599-642

[36] Visintin, A. *Differential models of hysteresis*, Springer

[37] Wiesen, K. and Charap, S. 1987 Vector Preisach modelling, J. Appl. Phys., 61, 4109-4021